

Optimization of Neon Soft X-ray Emission in Low Energy Dense Plasma Focus Device

M. A. Malek^{1,3}, M. K. Islam², M. Salahuddin¹

¹Jahangirnagar University, Savar, Dhaka, Bangladesh

²Plasma Physics Division, Atomic Energy Center, Dhaka, Bangladesh

³Green University, Dhaka, Bangladesh

E-mail: malekphy@gmail.com

Abstract: The Lee model code is used in numerical experiments for characterizing and optimizing neon soft X-ray (Y_{sxr}) yield of UNU/ICTP PFF machine operated at 14 kV and 30 μ F. The neon Y_{sxr} yield of the dense plasma focus device is enhanced by reducing static inductance (L_0) and anode length (z_0) along with increasing anode radius (a) and cathode radius (b), keeping their ratio ($c = b/a$) constant at 3.368. At the optimum combination of the electrodes geometry and static inductance, the maximum computed value of neon Y_{sxr} yield is 63.61 J at operating pressure 3.3 Torr with corresponding X-ray yield efficiency 2.16%, while the end axial speed becomes 6.42 cm/ μ s. This value of neon Y_{sxr} yield is twelve to thirteen times higher than the measured value (5.4 ± 1 J) at 3.0 Torr. It is also found that this neon Y_{sxr} yield is improved around seven times from previously computed value (9.5 J) at 3.5 Torr for optimum anode configuration of this machine. Our obtained results of neon Y_{sxr} yield are also compared with the computed results of AECS-PF2 machine operated at 15 kV and 25 μ F and is found that our results are about three times better than that from the optimized AECS-PF2 at $L_0 = 15$ nH.

Keywords: Dense Plasma Focus, Lee model code, Inductance, Electrode geometry, Neon soft X-ray.

1. Introduction

The dense plasma focus (DPF) device is a non-radioactive co-axial accelerator with relatively simple operating principle that produces a high-density, high-temperature plasma along with pulsed fusion neutron yield, soft and hard X-rays, high energy electron and ion beam, and electromagnetic waves [1,2,3]. This device is easy to construct, requires minimum maintenance and cost. The pulsed X-ray emitted from it is the highest among all other existing devices of equivalent operating energy [4]. The DPF device as high intensity pulsed X-ray source has a wide range of real life applications such as: X-ray spectroscopy [5], X-ray microscopy and lithography [6], X-ray laser pumping [7], X-ray crystallography [8], X-ray radiography [9], X-ray back-lighter [10] and X-ray micromachining [11]. The United Nations University/International Center for Theoretical Physics Plasma Focus Facility (UNU/ICTP PFF) is a 3.3 kJ Mather-type DPF machine which is switched on by a parallel-plate switching cascade air-gap, powered by 15 kV and 30 μ F Maxwell Capacitor [12]. The UNU/ICTP PFF machine has a unique contribution of plasma focus research. The UNU, ICTP and AAAPT (Asian African Association for Plasma Training) developed this device to initiate and promote practical knowledge and skills in plasma physics as well as fusion, in developing countries [13]. This machine produces realistic focusing action operating in several gases (He, Ne, Ar, H₂, CO₂, D₂, N₂ etc.) [14]. The neon Y_{sxr} yield for optimized DPF machine with operating energy from 0.2 kJ to 1 MJ was computed through numerical experiments by Lee model code and observed that the Neon is to be a suitable operating gas for the device as the source of soft X-ray yield [15].

The Lee model code is used to compute the realistic focus parameters along with the soft X-ray yield by only adjusting the computed discharge current wave trace with the experimentally measured one. In the case of NX2 DPF machine, this code has been successfully used showing a reasonable good agreement between the computed and measured values of neon Y_{sxr} yield as a function of pressure [4]. Therefore, the Lee model code is used to compute and optimize a DPF machine for improving the realistic Y_{sxr} yield.

For enhancing X-ray yields from the device, many efforts have been made by changing the bank, tube and operational parameters such as: energy of the bank static, circuit inductance, discharge current, electrode configuration (shape and materials) insulator materials and dimensions, gas composition, and filling gas pressure [16].

The measured value of neon Y_{sxr} yield from UNU/ICTP PFF was (5.4 ± 1) J at optimum pressure of 3.0 Torr with corresponding efficiency of 0.18% [2]. The numerical experiment on this device was carried out using Lee model code to compute the optimum neon Y_{sxr} yield keeping cathode radius ' b ' fixed at 3.2 cm, the anode length ' z_0 ' was drastically decreased from 16 to 7 cm, whilst the anode radius ' a ' was slightly increased from 0.95 to 1.2 cm from the standard configuration. As a result, the neon Y_{sxr} yield increased to 9.5 J at optimum pressure 3.5 Torr with corresponding efficiency of 0.32% [13]. This computed efficiency of Y_{sxr} was improved two to three times from the experimental value (0.18%) of the present UNU/ICTP PFF.

The AECS-PF2 is a 2.8 kJ Mather-type DPF machine operated with 15 kV and 25 μ F capacitor. Using the Lee model code, the reduction effect of static inductance (L_0) on neon Y_{sxr} yield from this device was investigated and optimized with electrodes geometry for maximum neon Y_{sxr} yield. At optimum configuration of AECS-PF2, the L_0 was reduced from 280 to 15 nH and hence the obtained neon Y_{sxr} yield was improved from its typical value 0.04 to 21 J at operating pressure of 2.8 Torr with corresponding efficiency of about 0.77% [16].

It is understood that the effect of L_0 on neon Y_{sxr} yield in optimization of UNU/ICTP PFF has not been done. Therefore, this device is optimized using Lee model code to enhance neon soft X-ray yield finding the optimum L_0 with its corresponding combination of electrode geometry (z_0 , ' a ' & ' b ').

In this paper, section 2 describes the Lee model code, section 3 describes the method of numerical experiment and the detailed descriptions of numerical experiment on UNU/ICTP PFF with neon gas is given in section 4. The section 5 explains the finding process of optimum static inductance with its corresponding electrode configuration for possible maximum neon soft X-ray yield in optimized UNU/ICTP PFF.

2. Lee Model Code

The electrical circuit and plasma focus dynamics, thermodynamics, radiations are coupled by 'Lee model code' which enables a realistic simulation that analyse all of the gross properties and performances of a DPF machine [17]. This code is used in the interpretation of experiments and design of a DPF [18]. An improved 5-phase code incorporating finite small disturbance speed, radiation and radiation-coupled dynamics was used [4] and was first web-published [19] in 2000. Plasma self-absorption was included [17, 19] in 2007 improving soft X-ray simulation in neon, argon and xenon among other gases. It has been widely used as a

complementary facility in several machines, such as: UNU/ICTP PFF [4, 12], NX1 and NX2 [4], DENA [19]. It has also been used in other machines for design and interpretation including sub-kJ DPF machines [20], FNII [21], the UBA hard X-ray source [22], KSU PF [23] and a cascading DPF [24]. Computed information from Lee model code includes: axial and radial speeds and dynamics [12, 23], focus pinch duration and dimensions, average pinch temperatures and densities, soft X-ray characteristics and yield [4, 13], optimization of machines [4, 12, 13, 17], and adaptation with Modified Lee (ML) model for Filipov-type DPF devices [19]. The reason of continuous development of the code for the last three decades is that there is no breakthrough to publish the basis and description of the model code; although many details in recent years, as they evolved, the Plasma Focus Studies Institute's website has been described [17]. The modified 6-phase version of the Lee model code RADPFV6.1b for Type-2 (high inductance DPF) machines which have been found to be incompletely fitted with the 5-phase model due to a dominant anomalous resistance phase [25]. The soft X-ray emission is calculated by subtracting the plasma self-absorption from the generated soft X-ray energy (line radiation), which mainly depends on the temperature and density. In the Lee model code, this effect is included for obtaining neon Y_{sxr} yield [17]. This effect is caused by the reabsorption of an emitted photon (in this case, the soft X-ray) from an atom/ion by another plasma component before escaping the plasma region, resulting in a lower radiation yield.

In the Lee model code, the rate of neon line radiation is calculated as follows [17]:

$$\frac{dQ_L}{dt} = -4.6 \times 10^{-31} n_i^2 Z Z_n^4 (\pi r_p^2) z_f / T \dots\dots\dots (1)$$

where, Q_L is the neon line radiation, Z_n is the atomic number, Z is the effective charge number, n_i is the number density, r_p the pinch radius, z_f is the pinch column length and T is the average temperature of pinch plasma. In the calculation of the code, Q_L is computed by integrating over the pinch duration. The neon soft X-ray yield is to be equivalent to the line radiation yield i.e., $Y_{sxr} = Q_L$ within the temperature range 200 – 500 eV (2.32×10^6 to 5.8×10^6 K) which corresponds to an end axial speed 6 - 7 cm/ μ s [2] at the modified 6-phase Lee model code.

3. Method of Numerical Experiment

The measured discharge current waveform is a significant indicator to realistically simulate and analyze all the gross performance of any DPF device. Important information such as: the axial and radial phase dynamics, temperature and thermodynamic properties, the crucial energy transfer into the focus pinch that causes nuclear fusion and hence the radiation yields from the device is carried out from the current waveform [18]. This is why the discharge current trace fitting is one of the best important techniques to optimize and configure a DPF. Therefore, the fitting of the computed discharge current waveform to the measured value through numerical experiment using Lee model code provides a lot of valuable insights of the pinched plasma. First of all, the measured data of the corresponding total discharge current waveform is collected either from laboratory experiment or picked out from published article. To start numerical experiments, the Lee model code is configured for any DPF by providing the tube parameters: z_0 , 'a' and 'b'; the bank parameters: L_0 , C_0 and stray circuit resistance r_0 and the operational parameters: V_0 , P_0 and the fill gas [1, 18]. Then the computed total discharge current waveform is fitted to the measured waveform by sequential adjustment of the four model parameters: mass swept-up factor (f_m), plasma current factor (f_c) in the axial phase and accordingly radial mass factor (f_{mr}), radial current factor (f_{cr}) in the radial phase. First initiative of fitting, the values of axial model parameters f_m and f_c are adjusted in such a manner that the rising slope of computed current trace and peak discharge current are reasonably agreed with the measured total current trace [1]. Then the radial model parameters f_{mr} , f_{cr} are varied until the computed slope and the deep fit with the measured values.

4. Numerical Experiments on UNU/ICTP PFF with Neon Filling Gas

To start the numerical experiments, the Lee model code (version: RADPFV6.1b) is configured for the UNU/ICTP PFF device with the following published parameters:

Bank parameters: static inductance $L_0 = 110$ nH, $C_0 = 30$ μ F and stray circuit resistance $r_0 = 12$ m Ω ; Tube parameters: cathode radius $b = 3.2$ cm, anode radius $a = 0.95$ cm, and anode length $z_0 = 16$ cm; Operation parameters: voltage $V_0 = 14$ kV and pressure $P_0 = 2.8$ Torr neon gas [13].

A measured discharge current waveform of the UNU/ICTP PFF at 14 kV and 2.4 Torr neon filling gas has been collected from the reference [26]. To obtain a reasonably good fit of the numerically computed total discharge current waveform to the measured waveform (Fig. 1), the following model parameters has been obtained: $f_m = 0.05$, $f_c = 0.7$, $f_{mr} = 0.2$ and $f_{cr} = 0.8$ [13]. These fitted values of the model parameters have been used for the computation of all

the discharges at pressures from 1.0 to 4.2 Torr, keeping fixed all of the mentioned above bank, tube and operation parameters [13]. From the computed results, it is noticed that the neon Y_{srx} yield increases with increasing gas pressure until it goes to the maximum value of about 3.92 J at $P_0 = 3.3$ Torr with corresponding efficiency of 0.13% after which it decreases with further rising of the pressure. At this optimum pressure, the end axial speed is $v_a = 5.4$ cm/ μ s, the total peak discharge current is $I_{peak} = 180$ kA, the pinch current is $I_{pinch} = 103$ kA and the focusing time is about 3.97 μ s. It is observed that the focusing time increases with increase in the gas pressure. This is because higher the gas pressure, lower the current sheath velocity in both axial and radial phases and hence focus time comes slower with increase in gas pressure.

The characteristics of the variation of neon Y_{srx} yield with pressure depend on two major factors. Firstly: at the optimum pressure, the present configuration of UNU/ICTP PFF generate the appropriate end axial velocity of about 5.4 cm/ μ s, which correspond to the pinch temperature of 2.04×10^6 K, which is very close to the correct pinch temperature range for neon gas [27]. Secondly: the radiation yield is proportional to the square of the plasma density. Therefore, when the pressure is increased from a low value, the density of the pinched radiating plasma increases as a result the X-ray emission increases. Thus, at very low pressure the pinch plasma density is too low whilst the pinch temperature is to be very high due to high current sheath velocity. On the other hand, at very high pressure the pinch plasma density would be high and the corresponding pinch temperature may be too low for low current sheath velocity. In both cases, the pinch temperature may be away from the temperature range and hence the emitted neon Y_{srx} yield is low. Therefore, there would be an optimum pressure at which the pinch temperature and the corresponding end axial velocity are within the expected range whilst the density is still high enough for getting maximum neon Y_{srx} yield as shown in Fig. 2.

The measured values of neon Y_{srx} yield from UNU/ICTP PFF have been obtained by Liu [2] using a five-channel p-i-n soft X-ray detector confirmed by a calorimeter. In this experiment, the maximum value of neon Y_{srx} yield from this device was found to be about (5.4 ± 1) J at the optimum pressure of $P_0 = 3.0$ Torr with corresponding efficiency of 0.18%. At this optimum pressure, the typical values of the end axial speed is $v_a = 5.7$ cm/ μ s, the total peak discharge current is $I_{peak} = 180$ kA, the pinch current is $I_{pinch} = 111$ kA.

In addition, many numerical experiments have been carried out to observe the effect of applied voltage on neon Y_{srx} yield from UNU/ICTP PFF with pressure. The variation of neon Y_{srx} yields with pressure from this device are plotted at applied voltages of 12, 13, 14 and 15

kV as shown in Fig. 3. From this figure, it is seen that at optimum pressure, the neon Y_{sxr} yield rises from 2.74 to 4.49 J with increasing the applied voltage from 12 to 15 kV. It is also noticed for all applied voltages, the general natures of the variation of neon Y_{sxr} yield with pressure are almost the same.

The electrode geometry of UNU/ICTP PFF has also been optimized with pressure through numerical experiments using Lee model code, keeping $c = b/a$ constant at 3.4 for enhancing neon Y_{sxr} yield. At this practical optimization, the anode length z_0 is shorten drastically from 16 to 7 cm, the anode radius ‘ a ’ is increased from 0.95 to 1.2 cm and the cathode radius ‘ b ’ is kept unchanged at its original value of 3.2 cm [13]. At this optimum configuration, the computed values of $v_a = 4.9$ cm/ μ s, $I_{peak} = 184$ kA, $I_{pinch} = 141$ kA and the neon Y_{sxr} yield is about 9.5 J at optimum $P_0 = 3.5$ Torr with corresponding efficiency of 0.32%.

It is understood from the above observations that the neon Y_{sxr} yield rises two to three times from the standard UNU/ICTP PFF anode to the optimum anode configuration and it may be caused due to the increase of pinch current from 103 to 141 kA. Therefore, it would be a suitable technique to enhance Y_{sxr} yield from further increase in I_{pinch} .

5. Soft X-ray Yield Versus Inductance and Electrode Geometry

To compute the optimum L_0 with its corresponding combination of electrode geometry (z_0 , ‘ a ’ and ‘ b ’) for maximum neon Y_{sxr} yield from the optimized UNU/ICTP PFF, the values of $C_0 = 30$ μ F, $V_0 = 14$ kV and $P_0 = 3.3$ Torr neon and also the model parameters are kept constant throughout the numerical experiments. In these experiments, for each value of L_0 the corresponding r_0 is computed so that the factor RESF (RESF = stray circuit resistance/surge impedance = $r_0/\sqrt{(L_0/C_0)}$) remains fixed at 0.2. Also, for each L_0 the anode and cathode radii are adjusted in such a manner that their ratio $c = b/a$ is constant at 3.368. In our numerical experiment, the value of L_0 was varied from 100 nH to 1 nH using Lee model code.

In our numerical experiments the following techniques are applied to get the optimum combination of (L_0 , z_0 , ‘ a ’ and ‘ b ’) for maximum neon Y_{sxr} yield [16]:

- (i) The P_0 is kept constant at 3.3 Torr for all values of L_0 and also the value of z_0 is fixed at a certain value with each value of L_0 .
- (ii) Then the ‘ a ’ and correspondingly ‘ b ’ are varied keeping $c = 3.368$, until the maximum neon Y_{sxr} yield is computed for the certain value of z_0 .
- (iii) The ‘ a ’ as well as ‘ b ’ are varied with different values of z_0 at each L_0 to obtain the optimum combination for maximum neon Y_{sxr} yield.

- (iv) After that another value of z_0 is chosen, the maximum neon Y_{sxr} yield is computed by varying ‘ a ’ and ‘ b ’ and so on, until we have had the optimum combination of z_0 , ‘ a ’ and ‘ b ’ for the best maximum neon Y_{sxr} yield at a fixed value of L_0 .
- (v) The above procedures are repeated for gradually smaller L_0 until it was reached to 1 nH.

The reduction effects of L_0 on the discharge current waveforms with time are observed as shown in the Fig. 4. It is noticed from this figure that peak discharge current (I_{peak}) comes earlier for each reduction of L_0 . For example: when $L_0 = 30$ nH, $I_{peak} = 318.45$ kA at 1.28 μ s, when $L_0 = 20$ nH, $I_{peak} = 368.11$ kA at 1.02 μ s, when $L_0 = 10$ nH, $I_{peak} = 453.91$ kA at 0.60 μ s, when $L_0 = 5$ nH, $I_{peak} = 508.44$ kA at 0.31 μ s and when $L_0 = 3$ nH, $I_{peak} = 623.21$ kA at 0.28 μ s. Therefore, the z_0 is needed to be reduced so that the time taken by the plasma current sheath to reach at the end of z_0 coincides with rising time of the I_{peak} for maximum energy transfer to the crucial pinch region. At the same time, because of reducing L_0 , the value of I_{peak} increased as a result ‘ a ’ as well as ‘ b ’ were necessarily increased leading to longer pinch length (z_{max}) and hence a bigger pinch inductance ($L_p = \frac{\mu}{2\pi} \times \ln \frac{b}{r_p} \times z_{max}$) is found [16]. Thus, the geometry of the machine moved from longer thinner (Mather-type) to shorter fatter (Filipov-type) one as shown in Fig. 5. From the careful observation of this figure it is seen that neon Y_{sxr} yields start to increase proportionally from around $z_0 = 4$ cm to maximum at $z_0 = 2.4$ cm and then start to decrease sharply.

The values of ‘ a ’ and corresponding ‘ b ’ is varied with different values of z_0 at each L_0 to compute the optimum combination of them for getting maximum neon Y_{sxr} yield, which corresponds closely to the largest I_{pinch} . The optimization of z_0 , ‘ a ’ and ‘ b ’ with each L_0 for possible maximum value of neon Y_{sxr} yield with corresponding efficiency (% of stored energy E_0 transfers into soft X-ray yield) is shown in Table 1. It is found from the table that I_{peak} increases with each reduction in L_0 with no sign of any limitation as a function of L_0 . Whereas, I_{pinch} also rises gradually with reduction of L_0 . Finally, I_{pinch} reaches to a maximum value of 223.94 kA at $L_0 = 10$ nH whilst the neon Y_{sxr} yield reaches to its maximum value beyond which I_{pinch} as well as Y_{sxr} start to decrease with further reduction in L_0 , but the ratio of I_{pinch}/I_{peak} drops progressively as L_0 decreases. Fig. 6 shows the limitation effect of L_0 on I_{pinch} and Y_{sxr} in UNU/ICTP PF operated with neon gas at 3.3 Torr, where L_0 is reduced from 100 nH to 1 nH. The following three reasons make the combined effect that limit the I_{pinch} accordingly neon Y_{sxr} yield at optimum combination of (L_0 , z_0 ‘ a ’ and ‘ b ’):

- (i) If L_0 is reduced to zero then I_{peak} would not be infinity because at $L_0 = 0$ though the surge impedance ($Z_0 = \sqrt{L_0/C_0}$) is zero, the dynamics of plasma current sheath produces an impedance, which then becomes the dominating load to limit the value of I_{peak} .
- (ii) The capacitor bank will discharge within a short time through the focus pinch as L_0 is reduced to a very small value and it becomes more and more immediately coupled to the pinch.
- (iii) The energy distributions and the requirement to adjust z_0 'a' as well as 'b', the situation requires that as L_0 is decreased, the ratio of I_{pinch}/I_{peak} reduces [28].

Looking at the table, it is also observed that as L_0 is reduced gradually and hence the corresponding 'a' as well as 'b' have to be increased, whereas z_0 decreased progressively to compute the optimum combination of (L_0 , z_0 'a' and 'b') for maximum neon Y_{sxr} yield. In addition, for each reduction of L_0 with its corresponding optimum combination of electrodes geometry the plasma pinch dimensions (pinch radius a_{min} and pinch length z_{max}) rise as a result the Y_{sxr} yield increases. This variation of optimum neon Y_{sxr} yield and its corresponding optimum combination of z_0 , 'a' and 'b' with L_0 is shown in Fig. 7.

In the table, the maximum value of neon Y_{sxr} yield with corresponding efficiency at optimum combination of static inductance and electrode geometry (L_0 , z_0 , 'a' & 'b') is represented by bold values. From this table, it is found that the maximum neon Y_{sxr} yield is 63.61 J with corresponding efficiency of 2.16% at optimum electrode geometry of $z_0 = 2.40$ cm, 'a = 2 cm' and 'b = 6.736 cm' with $L_0 = 10$ nH in the optimized UNU/ICTP PFF at 14 kV and 3.3 Torr neon.

The neon Y_{sxr} yield optimization for each value of L_0 , varying z_0 , 'a' and 'b' has also been observed in AECS-PF2 at 15 kV and 2.8 Torr neon [16]. It was computed the optimum static inductance and combination of electrode geometry as ($L_0 = 15$ nH, $z_0 = 2.24$ cm, 'a = 1.732 cm' and 'b = 5.83 = cm'), the maximum neon Y_{sxr} yield was found to be about 21.77 J is shown in Fig. 8.

It is also found from Fig. 9 that the efficiency of soft X-ray emission from UNU/ICTP PFF increases with reducing L_0 and z_0 . The efficiency is also higher for larger values of 'a' and 'b'. Accordingly, the maximum efficiency of neon Y_{sxr} yield from optimized UNU/ICTP PFF is around 2.16% at the corresponding end axial speed of 6.42 cm/ μ s.

Whereas, the efficiency of neon Y_{sxr} yield from AECS-PF2 at 15 kV and 2.8 Torr was found to be 0.77 % with the corresponding end axial speed of 5.15 cm/ μ s shown in Fig. 10. It is assessed from the numerical experiments that the efficiency of neon Y_{sxr} yield in optimized

UNU/ICTP PFF (2.16%) is almost three times greater than that in optimized AECS-PF2 (0.77%) shown in Fig. 11. The difference in efficiency of these two optimized DPF machines can be explained as:

- (i) The variation trend of z_0 , 'a' and 'b' with L_0 in both machines are same.
- (ii) The optimum values of 'a' for each L_0 in UNU/ICTP PFF is slightly larger than that in AECS-PF2.
- (iii) For each L_0 the optimum value of 'b' is significantly higher in UNU/ICTP PFF than that of AECS-PF2 as shown in Fig. 12.

As the values of 'b' is significantly large and 'a' is slightly high in optimized UNU/ICTP PFF, the pinch column length and duration of pinch are higher than those of AECS-PF2 and Y_{srx} is proportionally related to them. As a result, the neon Y_{srx} yield, as well as its corresponding efficiency at the optimum combination of (L_0 , z_0 , 'a' and 'b') in UNU/ICTP PFF about three times higher from the optimized AECS-PF2. Therefore, in optimization of AECS-PF2, it may have computed better result with more increase in electrode radius.

Based on the obtained results of these sets of numerical experiments with neon gas, we can say that to improve the neon Y_{srx} yield, L_0 should be reduced to a value around 10 – 20 nH, which is an achievable range incorporating low inductance technology (NX2 machine constructed with $L_0 = 20$ nH), below which the pinch current I_{pinch} and the Y_{srx} yield, as well as the corresponding efficiency would not be improved sufficiently, if at all. Moreover, the neon Y_{srx} yield may be improved twelve to thirteen times from the standard UNU/ICTP PFF by the remarkable increase in 'b' and 'a' with reducing z_0 and L_0 , keeping $c = b/a$ constant at 3.368 in the laboratory.

Conclusions

The Lee model code (version: RADPFV6.1b) is applied to characterize and optimize the UNU/ICTP PFF machine operated at 14 kV and 30 μ F as a source of neon Y_{srx} yield. The reduction effects of L_0 and the electrodes geometry (z_0 , 'a' and 'b') on the neon Y_{srx} yield is studied.

In our numerical experiments with this DPF machine, the neon Y_{srx} yield increases to 63.61 J at operating $P_0 = 3.3$ Torr with the corresponding efficiency of 2.16% at the optimum combination of ($L_0 = 10$ nH, $z_0 = 2.4$ cm, 'a = 2.0 cm' and 'b = 6.736 cm'). The limitation effect of L_0 on neon Y_{srx} yield is also observed from these numerical experiments. From the published paper, it is understood that the maximum measured neon Y_{srx} of UNU/ICTP PFF

machine was (5.4 ± 1) J at optimum pressure of $P_0 = 3.0$ Torr with corresponding efficiency of 0.18%. At the present configuration of the machine, the computed maximum neon Y_{sxr} yield was 3.92 J at optimum pressure of $P_0 = 3.3$ Torr with corresponding efficiency of 0.13%. On the other hand, at optimum anode configuration, neon Y_{sxr} yield was computed to 9.5 J at optimum pressure of $P_0 = 3.5$ Torr with corresponding efficiency of 0.32%. Our computed value of neon Y_{sxr} yield is twelve to thirteen times higher than the experimentally measured value.

This obtained result of neon Y_{sxr} yield and corresponding efficiency are also compared with the computed results of AECS-PF2 operated at 15 kV and 25 μ F. The values of ‘ a ’ and ‘ b ’ of our optimized UNU/ICTP PFF at $L_0 = 10$ nH are significantly larger than those for optimized AECS-PF2 at $L_0 = 15$ nH. This increase in electrodes radius in the optimized UNU/ICTP PFF improves the efficiency of neon Y_{sxr} yield about three times from the optimized AECS-PF2.

Acknowledgments

The authors would like to appreciate Prof. S. Lee for his valuable support through the workshop ‘NEWPF2016’. The authors are grateful to Prof. M. Akel for providing the relevant documents and information. Gratitude from the authors goes to Dr. M. A. Humayun and M. S. S. Chowdhury for their encouragements to run the research work.

References

- [1] Lee, S., Saw, S. H., Soto, L., Springham, S. V., & Moo, S. P. (2009). Numerical experiments on plasma focus neutron yield versus pressure compared with laboratory experiments. *Plasma Physics and Controlled Fusion*, 51(7), 075006
- [2] Liu, M. (1996). *Soft X-rays from compact plasma focus* (Doctoral dissertation).
- [3] Habibi, M., Amrollahi, R., & Etaati, G. R. (2010). Experimental study of hard X-ray emission with different anode tips in APF plasma focus device. *Journal of fusion energy*, 29(1), 49-54.
- [4] Lee, S., Lee, P., Zhang, G., Feng, X., Gribkov, V. A., Liu, M., & Wong, T. K. (1998). High rep rate high performance plasma focus as a powerful radiation source. *IEEE Transactions on Plasma Science*, 26(4), 1119-1126.
- [5] A. D. Cahill, D. A. Hammer, S. A. Pikuz, and T. A. Shelkovenko, “Comment on ‘A doubly curved elliptical crystal spectrometer for the study of localized x-ray absorption in hot plasmas’ [Rev. Sci. Instrum. 85, 103114 (2014)],” *Rev. Sci. Instrum.*,

- vol. 87, no. 10, p. 107101, 2016.
- [6] Hassan, S. M., & Lee, P. (2017). Pulsed Plasma Sources for X-ray Microscopy and Lithography Applications. In *Plasma Science and Technology for Emerging Economies* (pp. 269-292). Springer, Singapore.
- [7] Depresseux, A., Oliva, E., Gautier, J., Tissandier, F., Nejdil, J., Kozlova, M., & Kim, H. T. (2015). Table-top femtosecond soft X-ray laser by collisional ionization gating. *Nature Photonics*, 9(12), 817-821.
- [8] Miao, J., Ishikawa, T., Robinson, I. K., & Murnane, M. M. (2015). Beyond crystallography: Diffractive imaging using coherent x-ray light sources. *Science*, 348(6234), 530-535.
- [9] Hussain, S., Shafiq, M., Ahmad, R., Waheed, A., & Zakauallah, M. (2005). Plasma focus as a possible x-ray source for radiography. *Plasma Sources Science and Technology*, 14(1), 61.
- [10] Beg, F. N., Ross, I., Lorenz, A., Worley, J. F., Dangor, A. E., & Haines, M. G. (2000). Study of x-ray emission from a table top plasma focus and its application as an x-ray backlighter. *Journal of Applied Physics*, 88(6), 3225-3230.
- [11] Gribkov, V. A., Srivastava, A., Keat, P. L. C., Kudryashov, V., & Lee, S. (2002). Operation of NX2 dense plasma focus device with argon filling as a possible radiation source for micro-machining. *IEEE transactions on plasma science*, 30(3), 1331-1338.
- [12] Lee, S., Tou, T. Y., Moo, S. P., Eissa, M. A., Gholap, A. V., Kwek, K. H., & Zakauallah, M. (1988). A simple facility for the teaching of plasma dynamics and plasma nuclear fusion. *American Journal of Physics*, 56(1), 62-68.
- [13] Saw, S. H., Lee, P. C. K., Rawat, R. S., & Lee, S. (2009). Optimizing UNU/ICTP PFF plasma focus for neon soft X-ray operation. *IEEE Transactions on Plasma Science*, 37(7), 1276-1282.
- [14] Zakauallah, M., Alamgir, K., Shafiq, M., Sharif, M., Waheed, A., & Murtaza, G. (2000). Low-energy plasma focus as a tailored X-ray source. *Journal of fusion energy*, 19(2), 143-157.
- [15] Lee, S., Saw, S. H., Lee, P., & Rawat, R. S. (2009). Numerical experiments on plasma focus neon soft X-ray scaling. *Plasma Physics and Controlled Fusion*, 51(10), 105013.
- [16] Al-Hawat, S., Akel, M., & Lee, S. (2011). Numerical experiments on Neon soft X-ray optimization of AECS-PF2 plasma focus device. *Journal of fusion energy*, 30(6), 494.

- [17] Lee, S. (2014). Radiative Dense Plasma Focus Computation Package: RADPF. <http://www.plasmafocus.net>; <http://www.intimal.edu.my/school/fas/UFLF/> (archival websites).
- [18] Lee, S. (2014). Plasma focus radiative model: Review of the Lee model code. *Journal of Fusion Energy*, 33(4), 319-335.
- [19] Siahpoush, V., Tafreshi, M. A., Sobhanian, S., & Khorram, S. (2005). Adaptation of Sing Lee's model to the Filippov type plasma focus geometry. *Plasma physics and controlled fusion*, 47(7), 1065.
- [20] Soto, L., Silva, P., Moreno, J., Silvester, G., Zambra, M., Pavez, C., & Kies, W. (2004). Research on pinch plasma focus devices of hundred of kilojoules to tens of joules. *Brazilian journal of physics*, 34(4B), 1814-1821.
- [21] Acuna, H., Castillo, F., Herrera, J., & Postal, A. (1996). Int. Conf. Plasma Sci., Conf. Record, 127.
- [22] Moreno, C., Raspa, V., Sigaut, L., Vieytes, R., & Clause, A. (2006). Plasma-focus-based tabletop hard x-ray source for 50 ns resolution introspective imaging of metallic objects through metallic walls. *Applied physics letters*, 89(9), 091502.
- [23] Abdou, A. E., Ismail, M. I., Mohamed, A. E., Lee, S., Saw, S. H., & Verma, R. (2012). Preliminary results of Kansas State University dense plasma focus. *IEEE Transactions on Plasma Science*, 40(10), 2741-2744.
- [24] Lee, S. (1991). A sequential plasma focus. *IEEE transactions on plasma science*, 19(5), 912-919.
- [25] Lee, S., Saw, S. H., Abdou, A. E., & Torreblanca, H. (2011). Characterizing plasma focus devices—Role of the static inductance—Instability phase fitted by anomalous resistances. *Journal of fusion energy*, 30(4), 277-282.
- [26] <http://www.intimal.edu.my/school/fas/UFLF/machines/UNU.htm>
- [27] Bing, S. (2000). *Plasma dynamics and x-ray emission of the plasma focus* (Doctoral dissertation, PhD Thesis).
- [28] Lee, S., & Saw, S. H. (2008). Pinch current limitation effect in plasma focus. *Applied Physics Letters*, 92(2), 021503.

Table 1: The optimum combination of z_0 , 'a' & 'b' in each value of L_0 with their corresponding neon soft X-ray yield for UNU/ICTP PFF at fixed $c = b/a = 3.368$, $P_0 = 3.3$ Torr, $V_0 = 14$ kV and $C_0 = 30$ μ F:

L_0	z_0	a	b	I_{peak}	I_{pinch}	I_{pinch}/I_{peak}	v_a	a_{min}	z_{max}	Y_{srx}	Efficiency
nH	cm	cm	cm	kA	kA	-	cm/us	cm	cm	J	%
100	8	1.25	4.21	190.92	139.45	0.730	4.47	0.08	1.82	9.88	0.34
75	7	1.37	4.614	217.88	155.93	0.716	4.65	0.09	2.00	14.51	0.49
50	4.85	1.58	5.321	260.46	180.96	0.695	4.70	0.10	2.34	24.57	0.84
30	4.3	1.74	5.86	318.45	202.68	0.636	5.27	0.12	2.63	37.62	1.28
20	3.8	1.84	6.197	368.11	215.43	0.585	5.78	0.14	2.84	48.86	1.66
15	3.39	1.91	6.44	405.21	221.13	0.546	6.12	0.15	3.03	57.58	1.96
10	2.4	2.00	6.736	453.91	223.94	0.493	6.42	0.18	3.23	63.61	2.16
5	1.3	2.00	6.736	508.44	212.95	0.419	7.03	0.21	3.25	55.63	1.89
3	1.27	2.50	8.42	623.21	195.21	0.313	7.12	0.36	3.90	19.08	0.65
1	1.26	2.60	8.757	729.94	177.86	0.244	8.47	0.18	4.05	8.08	0.27

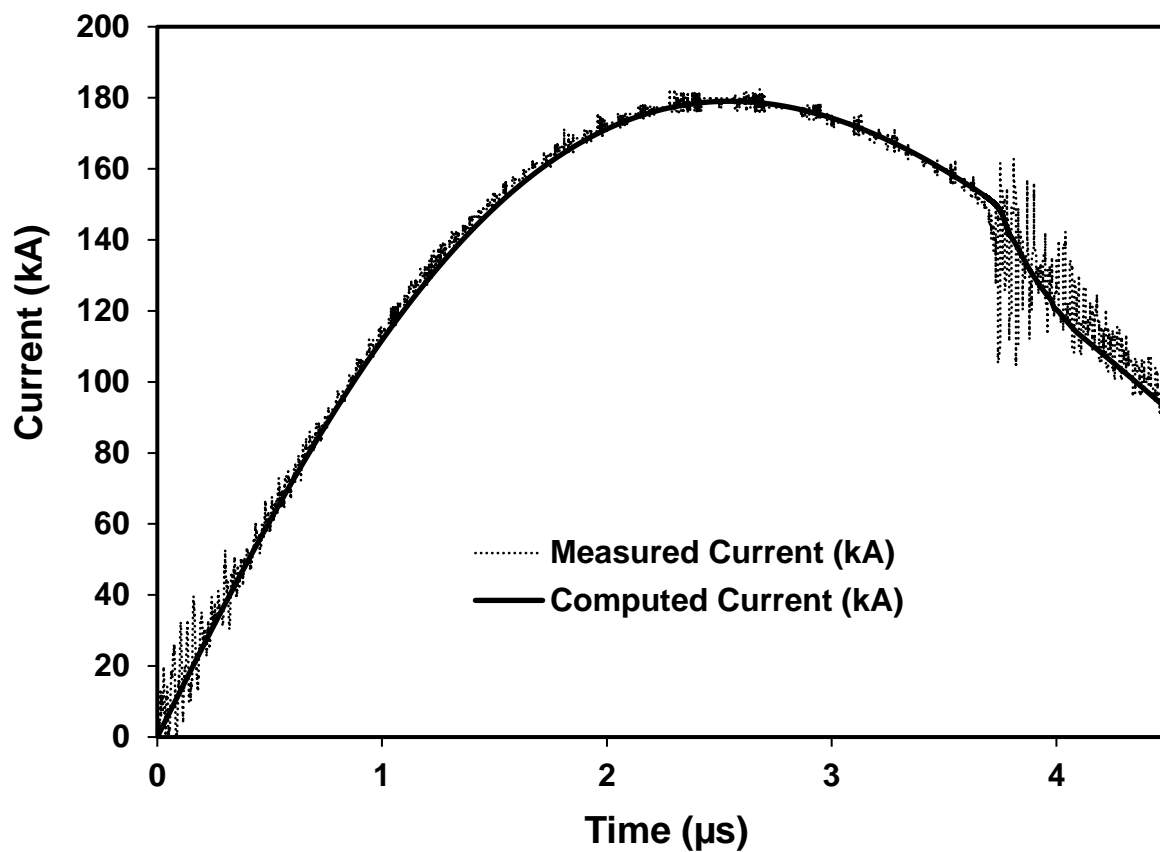


Fig. 1: Comparison of the experimental current waveform with the computed one of the UNU/ICTP PFF at 14 kV, 2.8 Torr with neon filling gas.

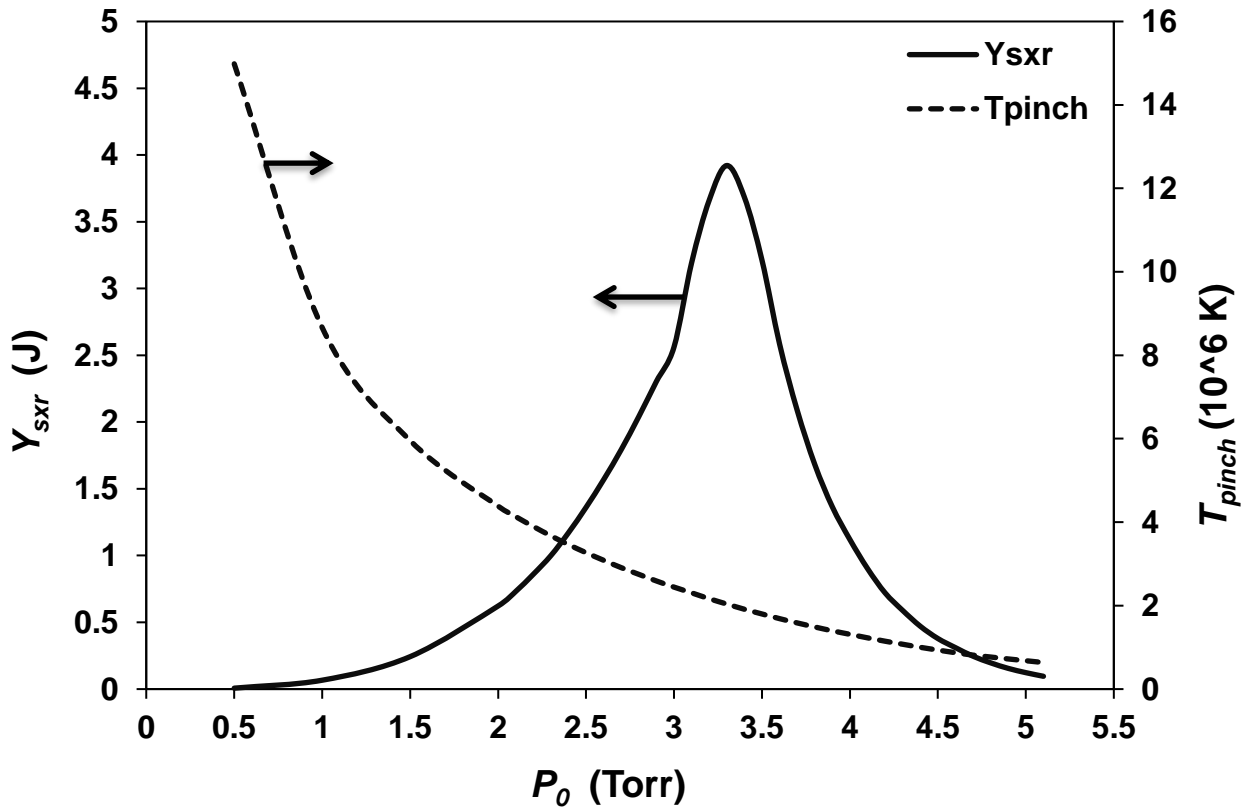


Fig. 2: Computed neon Y_{sxr} yield, plasma temperature with respect to pressure of UNU/ICTP PFF at 14 kV.

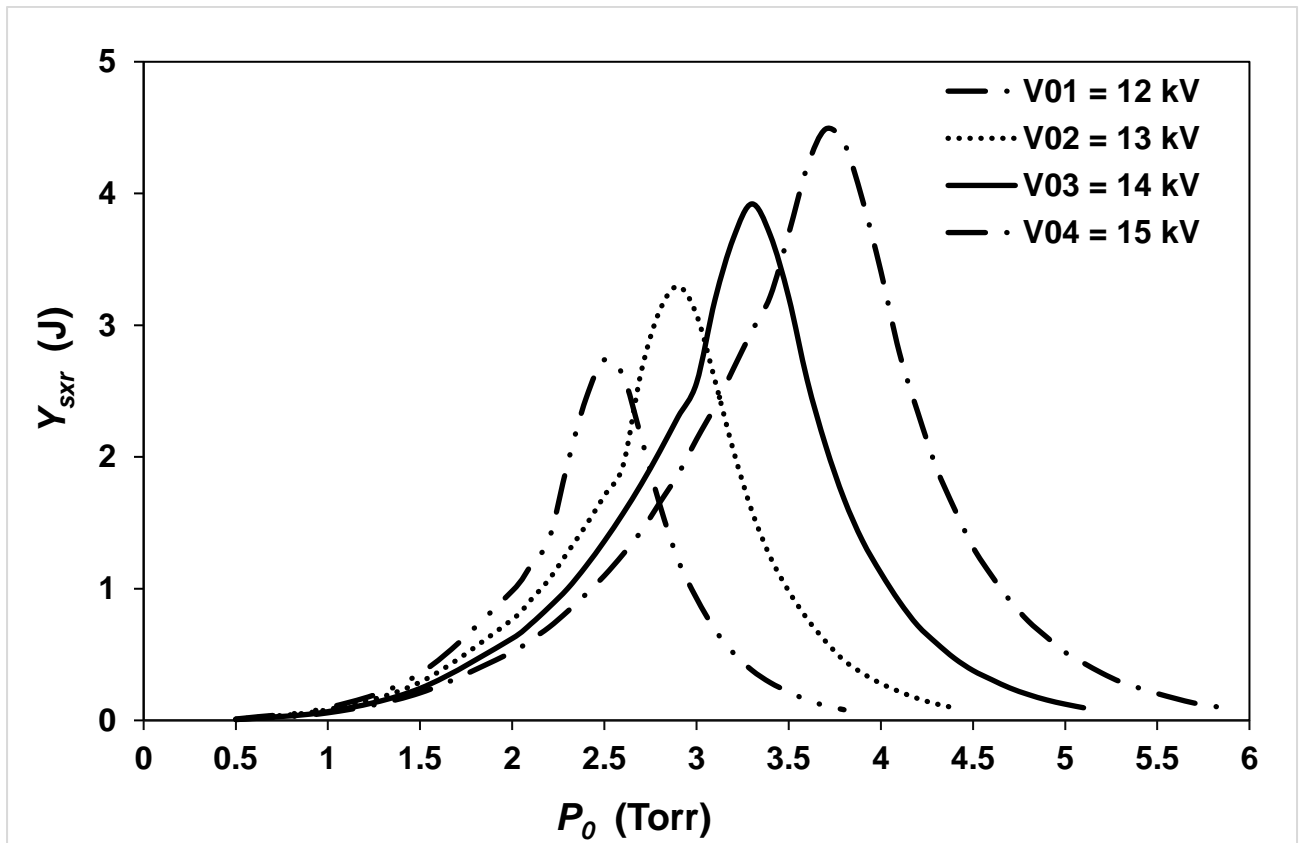


Fig. 3: Variation (computed) of neon Y_{sxr} yields from UNU/ICTP PFF with pressure at different applied voltages.

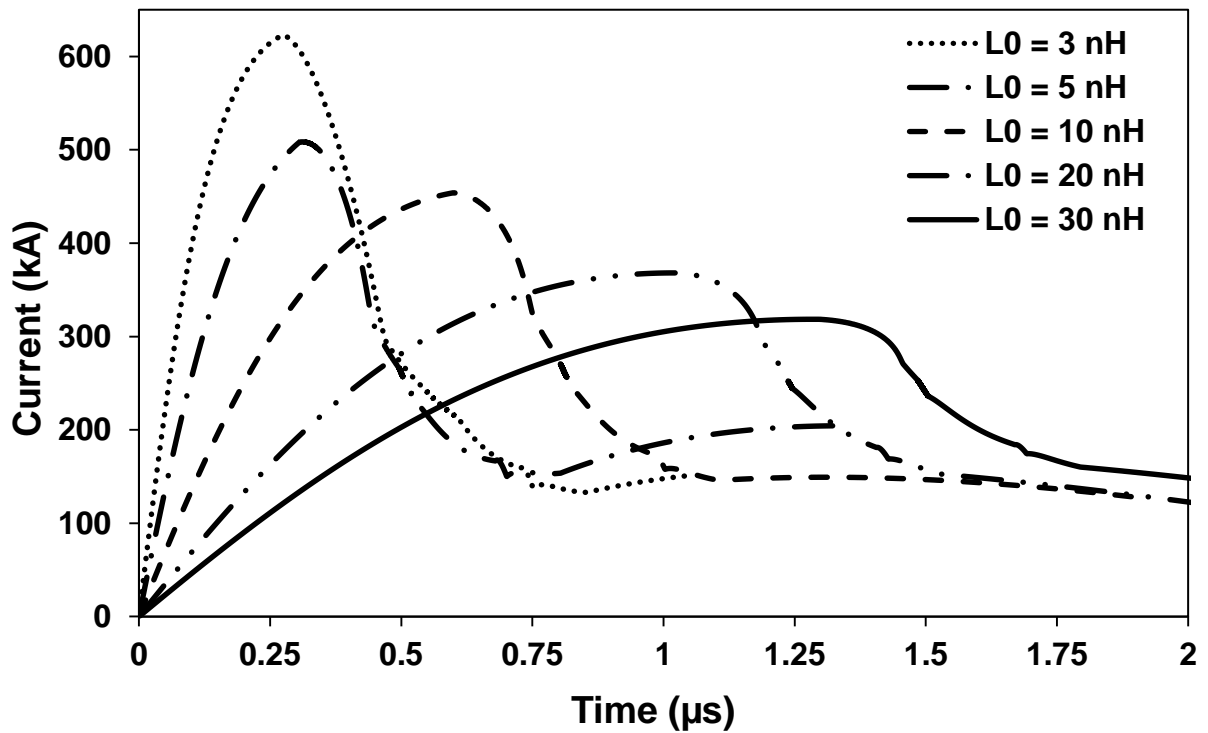


Fig. 4: Computed discharge current waveforms as a function of time from UNU/ICTP PF at 14 kV and 3.3 Torr neon with different values of L_0 .

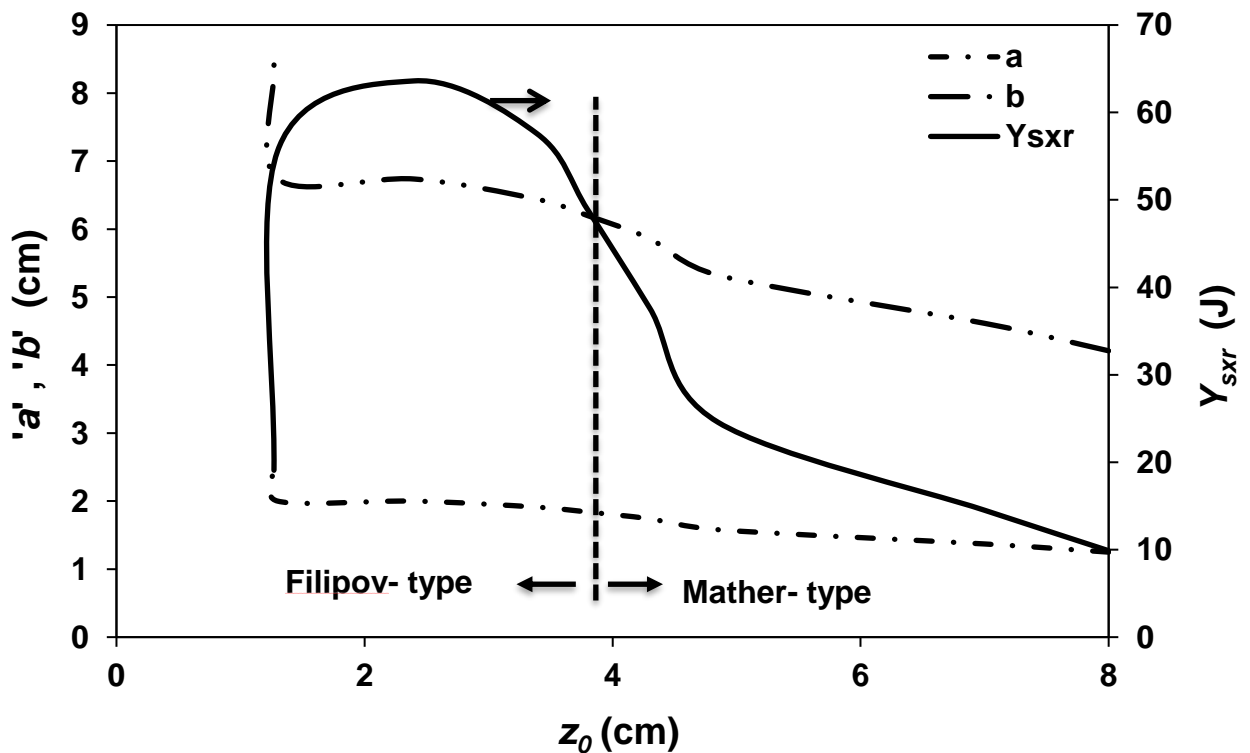


Fig. 5: Computed neon Y_{sxr} yield for each optimum combination of a and b with respect to z_0 from UNU/ICTP PFF at 14 kV and 3.3 Torr neon.

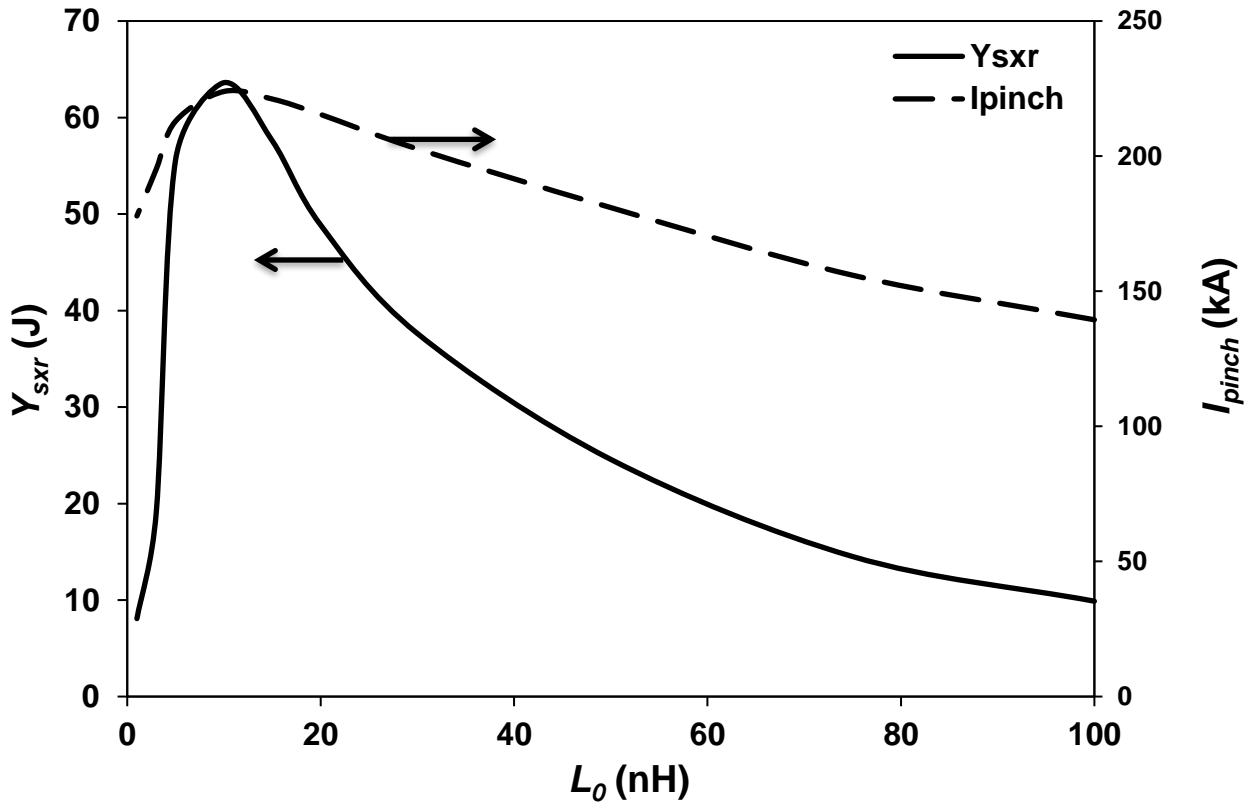


Fig. 6: Computed Y_{sxr} yield and I_{pinch} with respect to L_0 from UNU/ICTP PFF at 14 kV and 3.3 Torr neon.

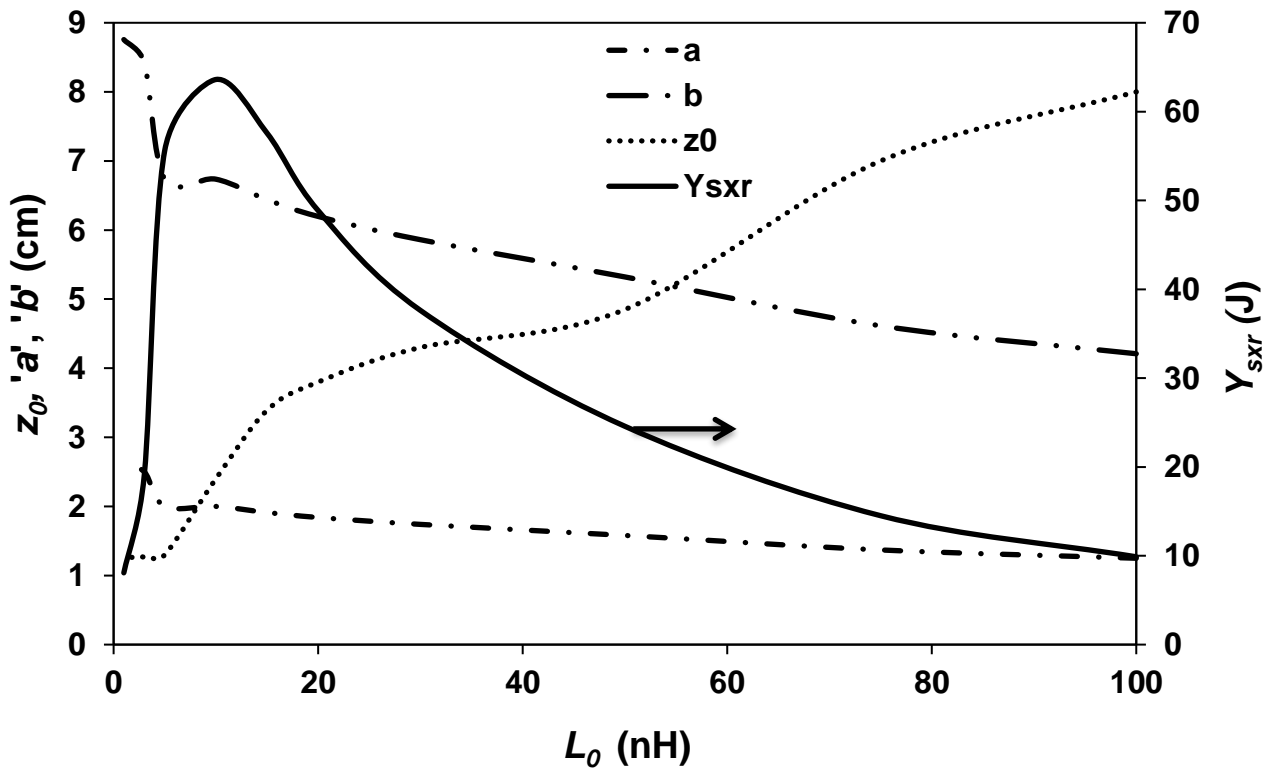


Fig. 7: Computed Y_{sxr} yields and its corresponding optimum electrode's geometry with respect to L_0 in UNU/ICTP PFF at 14 kV and 3.3 Torr neon.

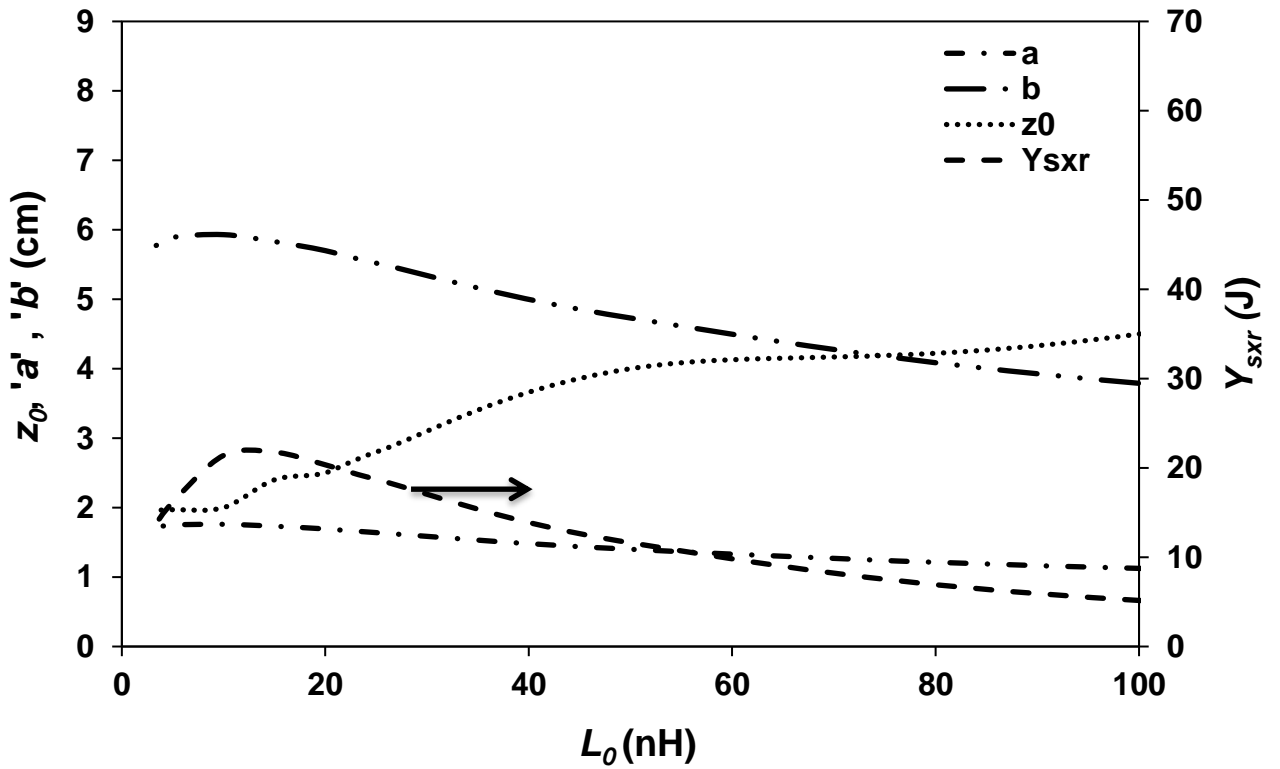


Fig. 8: Calculated Y_{srx} yields and its corresponding optimum electrode geometry with respect to L_0 in AECS-PF2 at 15 kV and 2.8 Torr neon.

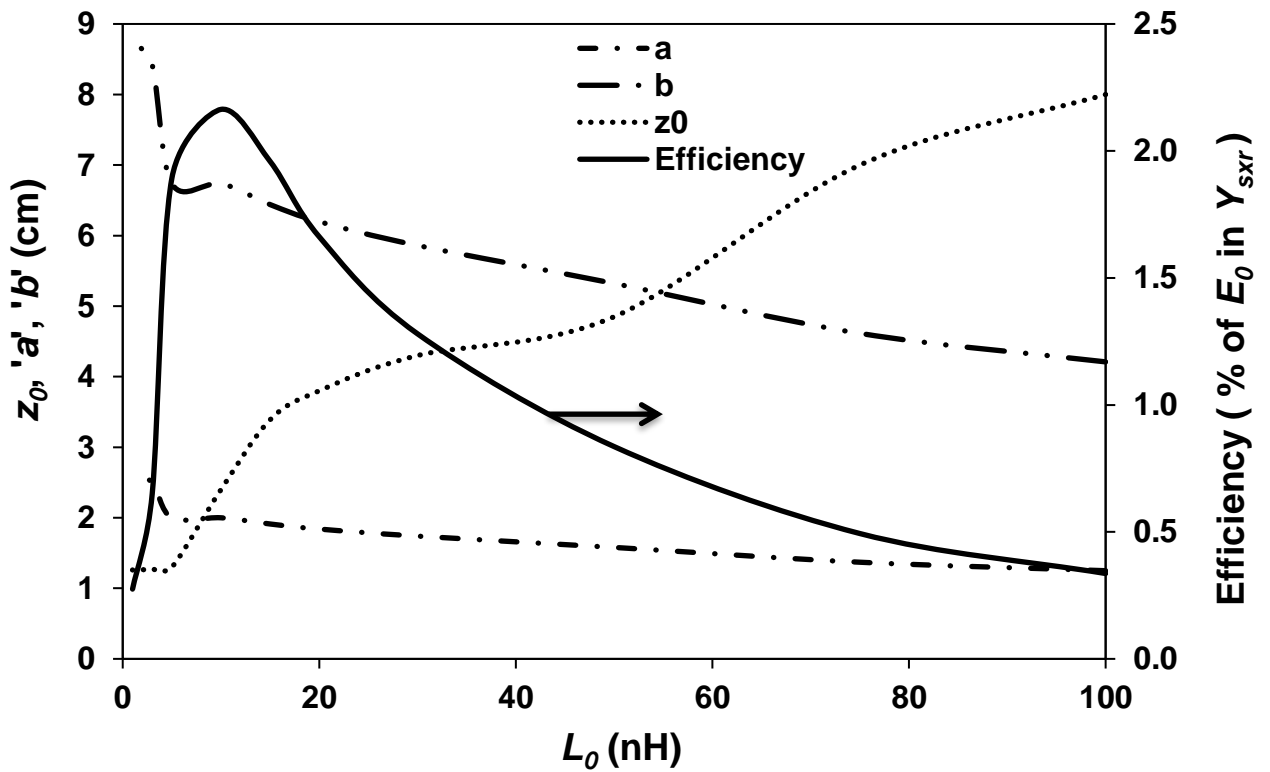


Fig. 9: Variation of efficiency (% of E_0 converted into Y_{srx}) and its corresponding optimum values of z_0 , 'a' and 'b' with L_0 in UNU/ICTP PFF at 14 kV and 3.3 Torr neon.

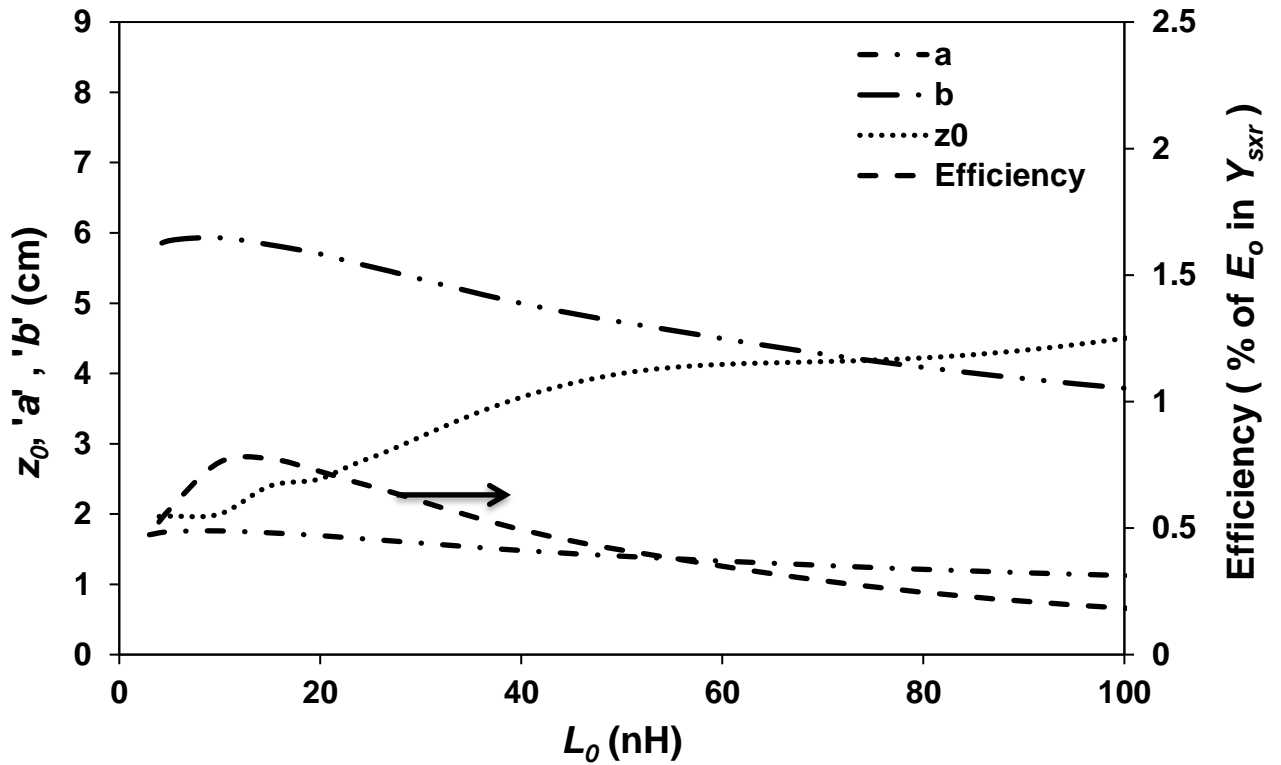


Fig. 10: Variation of efficiency and its corresponding optimum values of z_0 , $'a'$ and $'b'$ with L_0 in AECS-PF2 at 15 kV and 2.8 Torr neon.

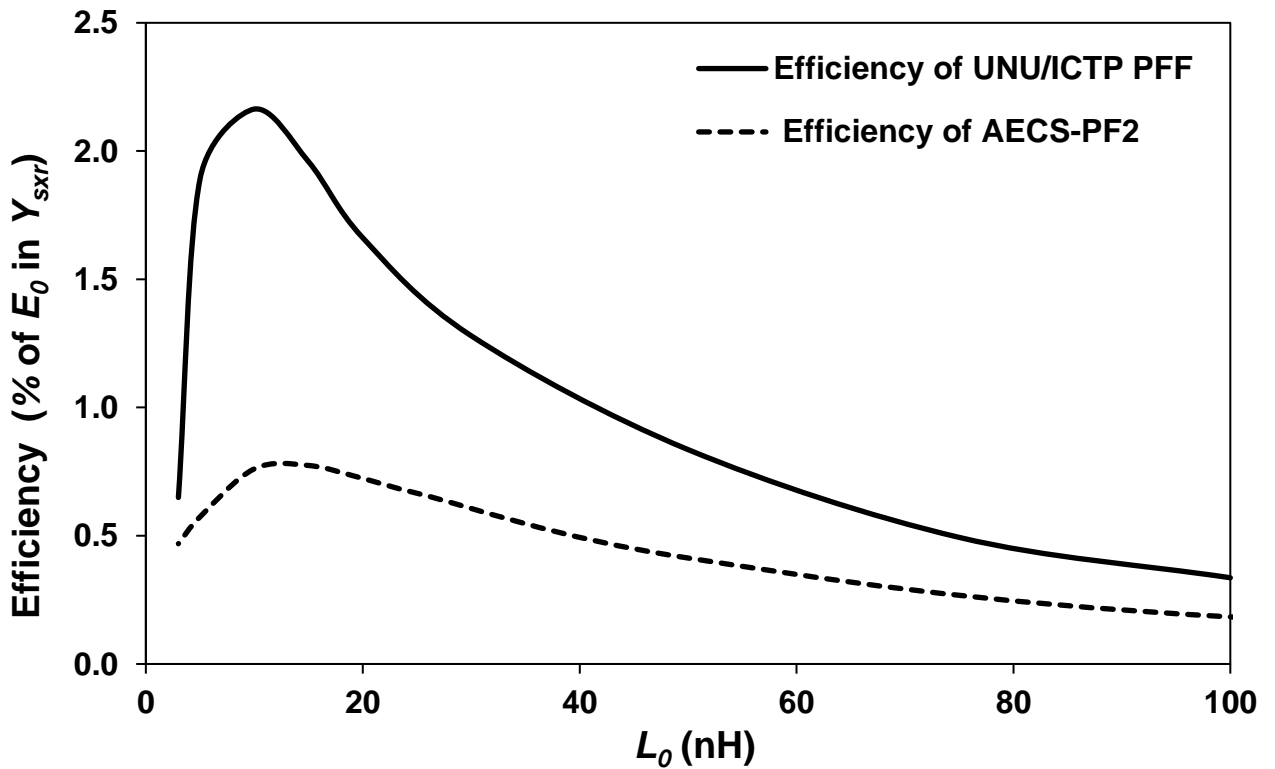


Fig. 11: Comparison of efficiency of UNU/ICTP PFF and AECS-PF2 devices at each optimum combination of electrode's geometry (z_0 , $'a'$ and $'b'$) with L_0 .

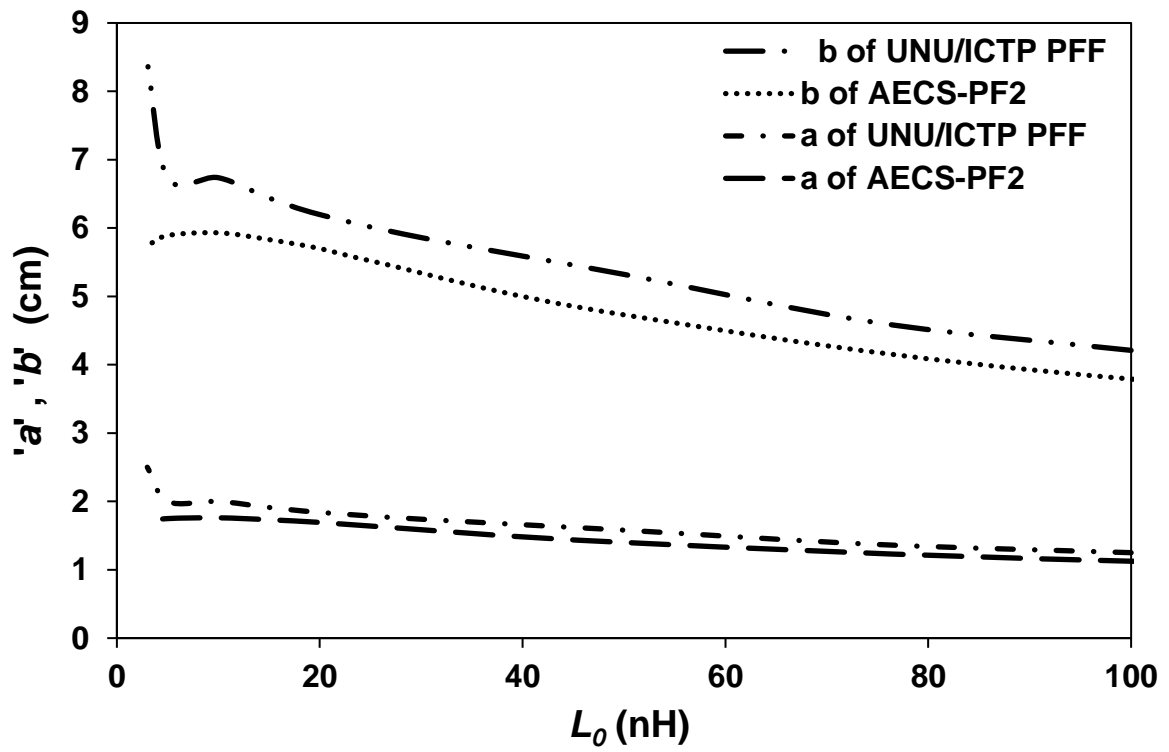


Fig. 12: Comparison of optimum electrode radius ('a' and 'b') for maximum neon Y_{svr} (computed) yields with L_0 for UNU/ICTP PFF and AECS-PF2.